NMR IN BIOMEDICINE
NMR Biomed. 2008; **21**: 265–271
Published online 5 July 2007 in Wiley InterScience
(www.interscience.wiley.com) DOI:10.1002/nbm.1189

Non-invasive measurement of brain viscoelasticity using magnetic resonance elastography

Ingolf Sack,[1] Bernd Beierbach,[1] Uwe Hamhaber,[2] Dieter Klatt[1] and Jürgen Braun[2]*

[1]Institute of Radiology, Charité - Universitätsmedizin Berlin, Berlin, Germany
[2]Institute of Medical Informatics, Charité - Universitätsmedizin Berlin, Berlin, Germany

Received 3 November 2006; Revised 16 March 2007; Accepted 4 May 2007

ABSTRACT: The purpose of this work was to develop magnetic resonance elastography (MRE) for the fast and reproducible measurement of spatially averaged viscoelastic constants of living human brain. The technique was based on a phase-sensitive echo planar imaging acquisition. Motion encoding was orthogonal to the image plane and synchronized to intracranial shear vibrations at driving frequencies of 25 and 50 Hz induced by a head-rocker actuator. Ten time-resolved phase-difference wave images were recorded within 60 s and analyzed for shear stiffness and shear viscosity. Six healthy volunteers (six men; mean age 34.5 years; age range 25–44 years) underwent 23–39 follow-up MRE studies over a period of 6 months. Interindividual mean ± SD shear moduli and shear viscosities were found to be 1.17 ± 0.03 kPa and 3.1 ± 0.4 Pas for 25 Hz and 1.56 ± 0.07 kPa and 3.4 ± 0.2 Pas for 50 Hz, respectively ($P \leq 0.01$). The intraindividual range of shear modulus data was 1.01–1.31 kPa (25 Hz) and 1.33–1.77 kPa (50 Hz). The observed modulus dispersion indicates a limited applicability of Voigt's model to explain viscoelastic behavior of brain parenchyma within the applied frequency range. The narrow distribution of data within small confidence intervals demonstrates excellent reproducibility of the experimental protocol. The results are necessary as reference data for future comparisons between healthy and pathological human brain viscoelastic data. Copyright © 2007 John Wiley & Sons, Ltd.

KEYWORDS: magnetic resonance elastography; brain; elasticity; shear modulus; shear viscosity; Voigt model; biomechanics

INTRODUCTION

The biomechanical properties of the brain have been the subject of many recent studies related to hydrocephalus (1–3), traumatic brain injury (4–6), and the evaluation of stroke or intraoperative evaluation (7,8). Most biomechanical tests were carried out by invasive indentation experiments (9,10) to specifically measure the elasticity of cortical brain tissue. In contrast, little is known about the viscoelastic properties of the bulk brain in its physiological environment. Elastography techniques have demonstrated for skeletal muscle (11–13), breast (14–19), and liver (20–25) that the elasticity of living tissue is sensitive to the development of pathologies and the degree of organ malfunction. In addition to elastic tissue behavior, viscose effects are considered to be a potential source of diagnostic information for differentiating benign and malignant breast tumors (26,27). These results have stimulated the search for biomechanical approaches that may support the diagnosis of neurological diseases.

Non-invasive assessment of brain stiffness requires the application of defined mechanical stress, which is naturally hampered by the mechanical shielding of the brain through skull, cerebrospinal fluid, and meninges. Nevertheless, it has been demonstrated that magnetic resonance elastography (MRE) (28–30) is capable of measuring two-dimensional (2D) (31–33) and three-dimensional (3D) (34–36) shear wave fields in brain induced by external actuators using vibration frequencies between 65 and 90 Hz. Most mechanical drivers are mounted to bite bars with individual denture molds. Here, a more generally applicable actuator is introduced that is better suited to clinical applications. Data acquisition in brain MRE is usually achieved by spin-echo or gradient-echo imaging techniques with extra motion-sensitizing gradients synchronized to the wave generator. Evaluation of wave data can be based on full 3D wave vector field inversion of the differential equation of motion or on equivalent inversion techniques adapted to 2D scalar wave fields (22,26,37–41).

In recent years, only a few MRE studies on human brain have been published; these show a great variety of shear modulus data, ranging from 2.5 to 15.2 kPa for white matter and from 2.8 to 12.9 kPa for gray matter

**Correspondence to:* J. Braun, Institute of Medical Informatics, Charité - Universitätsmedizin Berlin, Charité Campus Benjamin Franklin, Hindenburgdamm 30, 12203 Berlin, Germany.
E-mail: juergen.braun@charite.de
Contract/grant sponsor: Deutsche Forschungsgemeinschaft; *contract/grant number:* Br 2235/2-1, Sa 901/3-2.

Abbreviations used: 2D, two-dimensional; 3D, three-dimensional; EPI, echo planar imaging; MRE, magnetic resonance elastography.

(32,33,35). The variation in the results may have several reasons such as the dispersion of the shear wave speed at different excitation frequencies, a mismatch between wave propagation and image slice orientation in 2D MRE (36), varying wave amplitudes, and different boundary conditions. Brain MRE has not yet been assessed for its reproducibility and its potential to provide consistent results within one experimental study design. This article addresses this issue and proposes a protocol suitable for application of brain MRE to patients: examination times were reduced, patient comfort was increased, and the reproducibility of the experiment was tested in follow-up studies on six healthy volunteers lasting over several months.

The proposed technique is based on the fast acquisition of scalar wave fields using echo planar imaging (EPI) MRE. The wave excitation at 25 and 50 Hz is achieved by a redesigned head-rocker actuator, and analysis of wave data is based on complex-modulus inversion of time-resolved wave images. Shear moduli and shear viscosities are spatially averaged over gray and white matter. Therefore, they represent 'global' quantities with respect to the examined transverse slab through the ventricles. These data are intended for use as a reference for future brain MRE in patients performed with a similar experimental setup as that introduced in this study. Potential symptomatic changes in global brain visco-elasticity may then be attributable to diffuse effects of neurodegenerative diseases such as Alzheimer's disease and multiple sclerosis.

MATERIALS AND METHODS

Institutional review board approval was obtained, and written informed consent was obtained from all subjects. The experimental protocol was repeatedly applied over a period of 6 months to six healthy male volunteers aged 44, 36, 35, 34, 33, and 25 years (mean 34.5), henceforth labeled 1–6, respectively. The number of experiments varied between 23 (volunteer 6) and 39 (volunteer 5).

Wave image acquisition

All examinations were performed on a 1.5 T scanner (Magnetom Sonata; Siemens, Erlangen, Germany) using a standard head coil. A single-shot spin-echo EPI sequence was sensitized to motion by sinusoidal gradients of 40 ms duration and 35 mT/m amplitude. Either one or two bipolar cycles yielded a gradient oscillation synchronized to 25 Hz or 50 Hz vibration frequency (f), respectively (Fig. 1) (36). The direction of the motion-encoding gradient was toggled in subsequent image acquisitions to produce phase images with inverse motion contrast. Direction of motion encoding was in the slice selection direction, i.e. orthogonal to the image plane. The image slice position chosen was axial through the center of the brain within a slab of ~2 cm thickness. The bottom of the slab was positioned along the lower edge of the corpus callosum as demarcated in Fig. 2. Further acquisition parameters were: *TR* 3 s; *TE* 124 ms; field of view 192×192 mm; slice thickness 6 mm; in-plane resolution 1.5×1.5 mm.

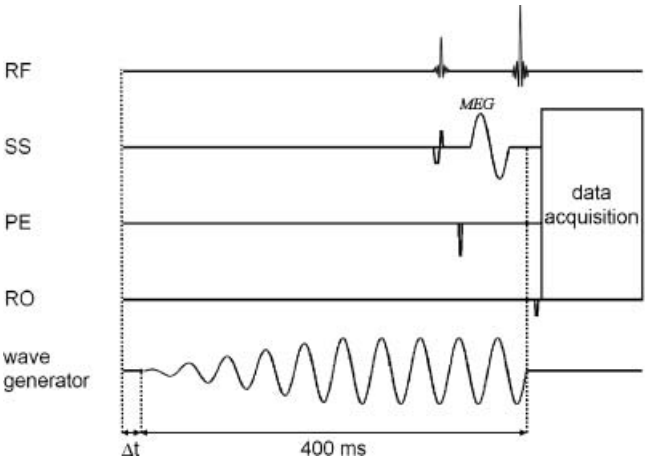

Figure 1. Diagram of the EPI MRE sequence used in this study. Radiofrequency pulses (RF), magnetic field gradients in the direction of slice selection (SS), phase encoding (PE) and read out (RO), and the wave generator output are shown schematically. Motion encoding is achieved using an oscillating motion-encoding gradient (MEG), here with one cycle of 25 Hz to encode corresponding tissue vibrations induced by a 10-cycle burst from the wave source. The trigger signal to the wave generator is given at begin of the pulse-sequence and consecutively shifted by a delay of Δt to gain temporal resolution in the measured wave data.

The trigger of the MRI sequence to the wave generator was $400\,\text{ms} + \Delta t$ before the start of motion encoding. Acquiring 20 phase images, Δt was increased 10 times either from 0 to 36 ms ($f = 25$ Hz) or from 0 to 18 ms ($f = 50$ Hz) in order to capture 10 time-resolved phase-difference wave images that displayed the propagation of the phase of the waves from 0 to $9/10 \times 2\pi$. The resulting total measurement time was 60 s. The amplitude of the output signal of the wave generator was increased linearly

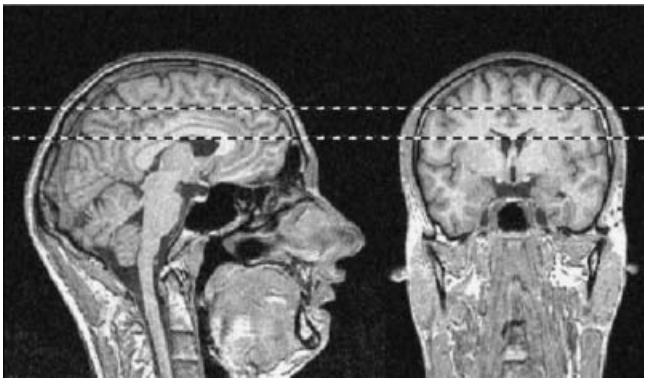

Figure 2. Approximated region (enclosed by dashed lines) of image slice positioning in planar MRE.

DOI: 10.1002/nbm

from 0 to its maximum in order to minimize mechanical transients on actuator and subjects (Fig. 1). Ten or 20 AC cycles were fed into the amplifier for 25 Hz or 50 Hz wave excitation, respectively.

Motion generation

Shear wave vibrations were produced by a remote motion generator based on a commercial loudspeaker (22). A flexible joint mounted in the center of the loudspeaker membrane was coupled via a carbon fiber rod of variable length (2–3 m) to a pin joint on top of a head rocker. The head rocker was built from a plastic tube with 235 mm diameter and 160 mm length, allowing its installation into a standard MRI head coil. The plastic tube was connected to a relocatable base plate with embedded cylindrical pivot. Two cylindrical rolls were used as a counter bearing attached to the base of the MRI head coil. The actuator setup is illustrated in Fig. 3. Maximum deflection amplitudes on the head surface were estimated to be 0.3–0.5 mm.

Motion measurement

A head phantom was constructed to measure the surface acceleration of a skull-shaped object inside the transducer. Therefore, a melon was attached to a stiff plastic tube with 1.5 m length and 12 cm diameter and fixed by Velcro strips to the MRI table. The supporting point of the phantom was subsequently moved in head–feet direction throughout the head rocker, while the deflections on the vertex were probed by a custom-built piezoelectric accelerometer. Three piezoelectric ceramic discs were orthogonally mounted and adjusted for measurement of the acceleration components in head–feet, anterior–posterior, and left–right direction. Data were sampled and stored by a digital oscilloscope (TDS 1002; Tektronix, Beaverton, OR, USA).

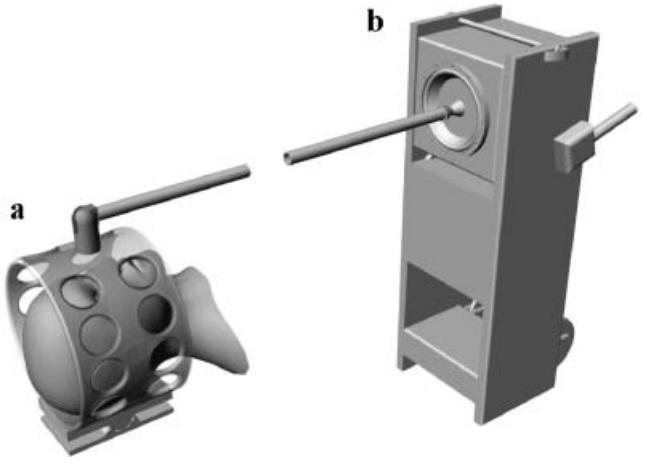

Figure 3. Head rocker unit (a) and remote vibration generator (b) used for shear wave excitation of the human brain. The length of the rigid rod that connects a and b was 2.8 m.

Data analysis

Phase-difference images were unwrapped and temporally Fourier-transformed. The resulting complex wave image at excitation frequency in the Fourier domain was further processed using a spatial Butterworth bandpass filter with lower and upper thresholds of 2.0 and 10.0 cm ($f = 25$ Hz) and 1.0 and 10.0 cm ($f = 50$ Hz) wavelengths, respectively. A complex wave image inversion was performed, yielding a complex modulus $G = G' + iG'' = \mu + i\eta\omega$ as described by Klatt *et al*. (22) and similar to approaches of other researchers (26,38). The assignments of shear modulus (μ) to the dynamic modulus (G'; real part of the complex modulus) and shear viscosity (η) to the loss modulus (G''; imaginary part of the complex modulus) divided by the angular driving frequency ($\omega = 2\pi f$) are based on Voigt's model of viscoelasticity (42). The density of the brain was assumed to be 1000 kg/m^3. μ and η were averaged over a spatial region of interest that was previously determined by manually segmenting the outer boundaries of the brain excluding ventricles.

RESULTS

Figure 4 shows experimental acceleration components as a function of head position. Moving the phantom about

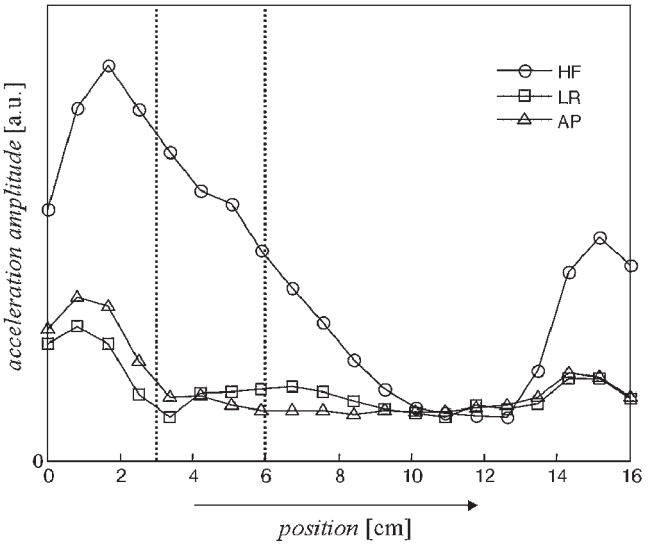

Figure 4. Position dependency of acceleration components on top of a head phantom (simulating forehead surface deflections). Relative acceleration amplitudes were measured in terms of voltages generated by piezoelectric accelerometers. In further *in vivo* experiments, the back of the head was positioned within the range marked by the dashed lines. HF, Head–feet direction; AP, anterior–posterior direction; LR, left–right direction.

DOI: 10.1002/nbm

16 cm between the two openings of the head rocker causes large variations in the measured amplitudes. Two principal findings are immediately apparent: (i) the main acceleration and thus also the main deflection component is parallel to the head–feet direction; (ii) this component has its minimum approximately at the position of the pivot of the head rocker. Therefore, in subsequent volunteer studies, the supporting point of the back of the head was placed off center in the range 3–6 cm according to Fig. 4. Moreover, motion encoding was adjusted along the direction of slice selection in order to capture the major component of the strain wave field.

Figure 5 shows example wave images acquired for volunteer 1 during different examinations at 25 Hz and 50 Hz vibration frequency. The experiments were performed by different operators with an interval of several days resulting in a variation in the image slice position within the slab demarcated in Fig. 2. Wave patterns vary visibly, which is presumably the result of the variation in the head position relative to the head rocker combined with a change in the kinetic freedom of the head due to muscle tension throughout the body. Generally, the lowest deflection amplitudes were found in the vicinity of the center axis of the brain in the left–right direction. This effect is attributed to a predominant nodding motion, with highest deflections at the forehead and at the back of the head.

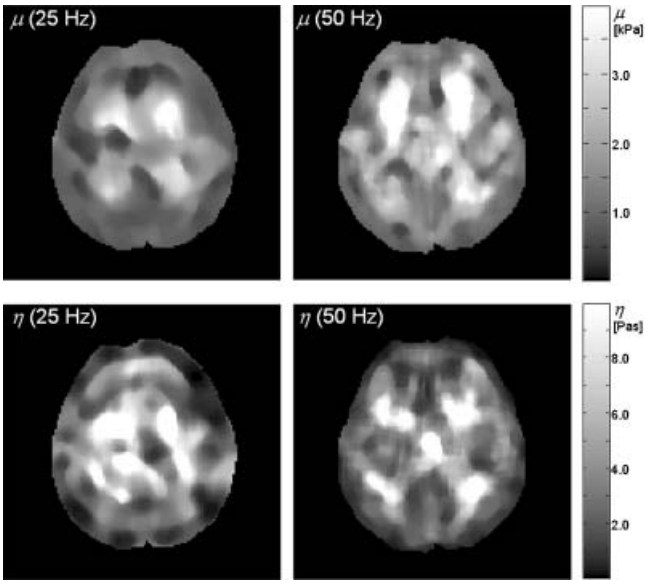

Figure 6. Elasticity (top row) and viscosity (bottom row) maps for volunteer 1 at excitation frequencies of 25 Hz and 50 Hz. Gray scale bars correspond to shear moduli of 0–4 kPa and shear viscosities of 0–10 Pas.

Example elasticity and viscosity maps calculated by complex wave image inversion are depicted in Fig. 6. Regions in the vicinity of the brain surface appear to be softer than central brain parenchyma, which supports

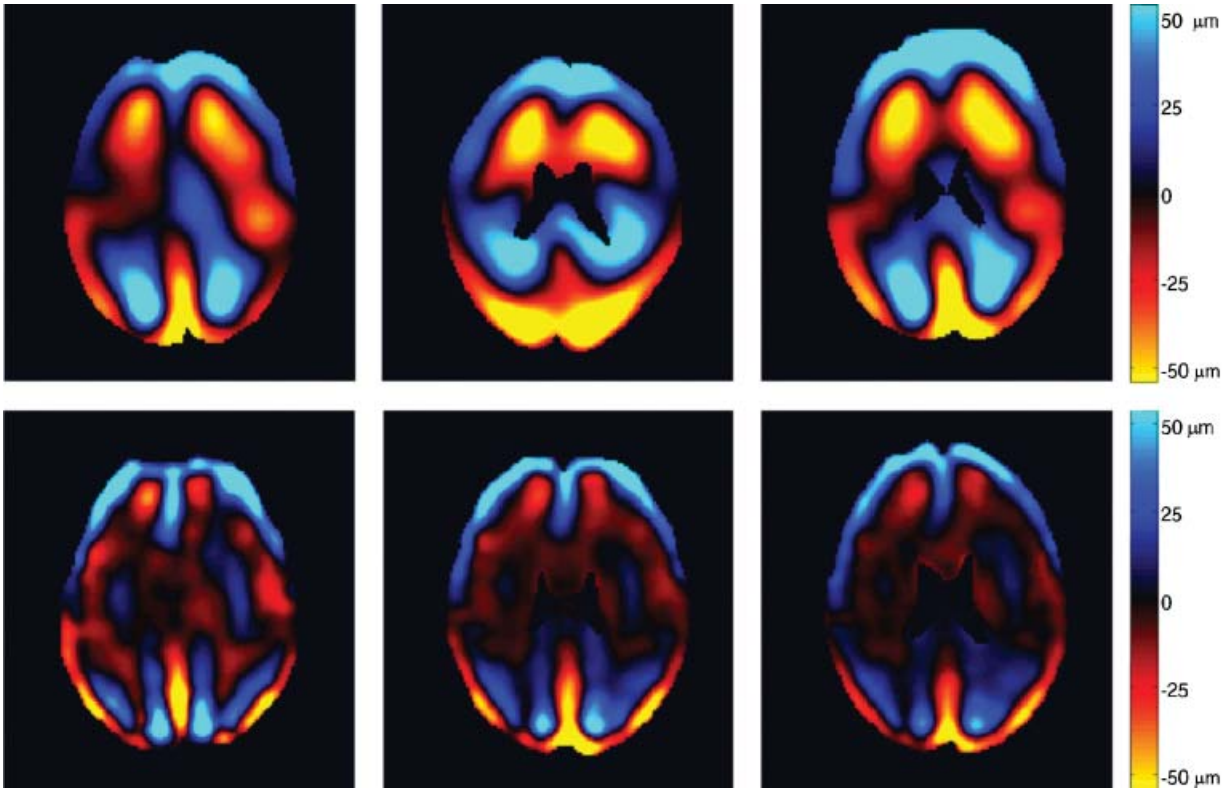

Figure 5. Example phase-difference shear wave images acquired in volunteer 1 on different days at an excitation frequency of 25 Hz (top row) and 50 Hz (bottom row). The experimental parameters of image slice position, head position, and amplifier output were slightly different, causing variable patterns. The color bar corresponds to deflection amplitudes of ± 50 μm.

DOI: 10.1002/nbm

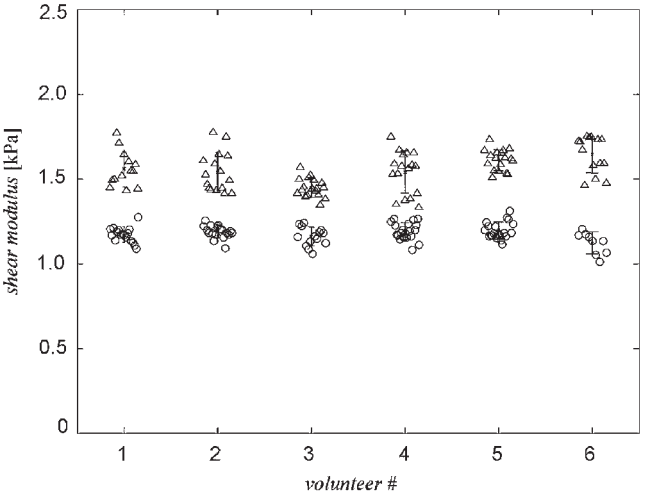

Figure 7. Experimental data for shear moduli with error bars assigned to the standard deviation of each volunteer data cluster at 25 Hz (circles) and 50 Hz (triangles) wave excitation.

observations (32,33) that white brain matter is stiffer than gray matter. However, according to the literature, shear waves near the surface are affected by diffraction or non-evanescent (non-propagating) waves, eventually leading to biases in the estimated local wavelengths (43–46). This conclusion justifies our approach of focusing on global measures, as shown in Figs. 7 and 8. There, the interindividual mean of $\mu = 1.17 \pm 0.03$ kPa at 25 Hz and $\mu = 1.56 \pm 0.07$ kPa at 50 Hz shows that the shear modulus is about one-third higher with higher vibration frequencies. In contrast, no dispersion was observed for the shear viscosity with mean values of 3.1 ± 0.4 Pas and 3.4 ± 0.2 Pas at 25 and 50 Hz, respectively. Interindividual shear modulus data are confined to 1.01–1.31 kPa at 25 Hz and 1.33–1.77 kPa at 50 Hz. Shear viscosity data range from 2.1 to 4.6 Pas and from 2.5 to 4.2 Pas at 25 Hz and 50 Hz excitation frequency, respectively. Intra- and interindividual means and standard deviations are listed in Table 1.

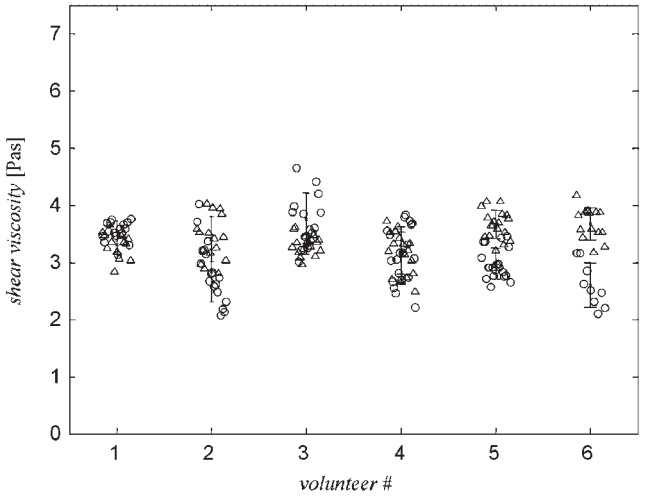

Figure 8. Experimental data for shear viscosity acquired at 25 Hz (circles) and 50 Hz (triangles) mechanical excitation frequency. The error bars correspond to the standard deviations of the data for each frequency and volunteer.

Table 1. Intraindividual means of the global viscoelastic data for volunteers 1–6 and corresponding interindividual average at 25 Hz and 50 Hz mechanical excitation frequencies. The error tolerances (±) are given as standard deviations

	μ (kPa)		η (Pas)	
Volunteer	25 Hz	50 Hz	25 Hz	50 Hz
1	1.17 ± 0.04	1.56 ± 0.1	3.5 ± 0.2	3.3 ± 0.2
2	1.19 ± 0.04	1.54 ± 0.12	2.8 ± 0.5	3.4 ± 0.4
3	1.16 ± 0.06	1.45 ± 0.06	3.8 ± 0.5	3.3 ± 0.2
4	1.19 ± 0.05	1.54 ± 0.13	3.1 ± 0.5	3.2 ± 0.4
5	1.2 ± 0.05	1.61 ± 0.06	3.0 ± 0.3	3.7 ± 0.2
6	1.12 ± 0.07	1.64 ± 0.11	2.6 ± 0.4	3.7 ± 0.3
1–6	1.17 ± 0.03[a]	1.56 ± 0.07[a]	3.1 ± 0.4[a]	3.4 ± 0.2[a]

[a]Here, standard deviations correspond to confidence intervals with $P \leq 0.01$.

DISCUSSION

We have demonstrated that viscoelastic constants of the human brain can be rapidly and reliably obtained using planar EPI MRE. Because this study focused on global viscoelastic constants, no intracranial heterogeneity was taken into account. Although this simplification neglects potentially valuable information on tissue heterogeneity, it also mitigates the aforementioned wave field biases near the tissue surface. Thus, the determined shear moduli displayed only small deviations of 2.5% (25 Hz) and 4.5% (50 Hz) despite apparent intraindividual variations in the wave patterns (Fig. 5).

The single-slice approach was driven by time considerations. It was shown by Hamhaber *et al*. (36) that there is a region where a geometrical overestimation of shear wave lengths is minimized (<10%). In this study, this region was chosen for the transverse image plane position. To further limit acquisition time, scalar wave fields were captured assuming isotropy of brain elasticity. Neglecting compression and evanescent (non-propagating) waves, this assumption predicts identical wavelengths in each component of the vector field. For this reason, any direction component of the strain wave field can be chosen for a scalar wave inversion. However, it should be noted that the amplitudes of shear waves with in-plane polarization are partially obliterated along the direction of wave excitation (46). In planar MRE, it is therefore desirable to capture through-plane shear waves which do not obey those constraints. Thus, our current nodding motive actuator, which mainly induces head–feet deflections, determines the transverse image plane used.

Figure 8 indicates that the viscosity (η) is non-dispersive in the examined frequency range, which

DOI: 10.1002/nbm

supports the attribution of η to G''/ω. Assigning μ to G' yields a frequency dependency of the shear modulus as shown in Fig. 7. The difference between shear modulus data for 25 Hz and 50 Hz vibration frequency (of the order of 0.4 kPa) is presumably the result of the inadequacy of Voigt's model for predicting the behavior of viscoelastic brain tissue. The Kramers–Kronig relation predicts a relation between dynamic modulus and loss modulus (43). Thus, treating G' separately from G''/ω disobeys this relation. On the other hand, the loss modulus inherently bears a larger error after inversion, as indicated by the standard deviations given in Table 1. Therefore, a separate view on G' yields a smaller error than when G' and G'' are combined, as required by more elaborate viscoelastic models. As a preliminary approach to compensating for dispersion, one could add a simple frequency-dependent correction term such as λ/ω to μ. With $\lambda \approx 120$ kPa/s, both 25 Hz and 50 Hz shear moduli data are increased to a common range between 1.7 and 2.2 kPa. Although such correction is not supported by rheological models, it may help to eliminate dispersion and thus to potentially increase the significance of relative, symptomatic variations in future brain MRE studies.

Without assuming any particular dispersion relation, it is important to consider the frequency range when comparing our own results with data from the literature. Using oscillation shear tests on porcine brain specimen, G' and G'' were reported in the frequency range 25–50 Hz by Nicolle *et al*. (47), Arbogast and Margulies (48), and Brands *et al*. (5) with dynamic moduli from 4.9 to 5.7 kPa, 1.0 to 1.2 kPa, and 0.8 to 0.9 kPa and loss moduli from 1.0 to 1.1 kPa, 0.5 to 0.9 kPa, and 0.4 to 0.5 kPa, respectively. Fallenstein *et al*. (49) investigated human white matter samples with 10 Hz shear oscillations, finding a loss modulus of 0.95 kPa and a dynamic modulus of 0.47, and Shuck and Advani (50) found dynamic moduli from 10.5 to 18.0 kPa and loss moduli from 5.0 to 9.0 kPa between 25 and 50 Hz. Our results for 25 Hz ($G' = 1.17 \pm 0.03$ kPa, $G'' = 0.49 \pm 0.06$ kPa) are within the interindividual standard deviations of Fallenstein *et al*. (49) despite the higher vibration frequency used. However, our data show a higher degree of dispersion than most data from the literature (except those of Shuck *et al*. (50)). We attribute this difference to either intrinsic differences between *ex vivo* and *in vivo* tests or a systematic misinterpretation of shear-wave patterns related to data postprocessing in MRE. One relevant point discussed in the literature is the treatment of hydrostatic compression in the inversion technique (26,39–41). Spatial filters as used here may decrease the determined shear moduli. However, a comparison with 3D MRE studies on human brain indicates that our data can extrapolate the dispersion given by the data of Green *et al*. (35) (2.5 kPa at 65 Hz) and Hamhaber *et al*. (36) (3.5 kPa at 83 Hz) to a static modulus (at 0 Hz) of ~0.8 kPa. This is even more notable because different inversion techniques have been used in both studies that are less sensitive to compression waves than the method introduced here.

In summary, an experimental protocol based on 2D EPI MRE combined with a head-rocker actuator is introduced for the fast measurement and reproducible determination of viscoelastic constants of living human brain. With this protocol, averaged shear modulus and shear viscosity data of the cerebrum were obtained in six healthy male volunteers that show no significant interindividual variation. Repetitions of the experiment over a longer time period illustrated the stability of scalar wave field analysis against variations in shear wave patterns that may occur if the relative positions between volunteer, actuator, and image plane are changed slightly. The results of this study represent the first comparison of brain viscoelastic data between healthy subjects. The given viscoelastic parameters may be useful for relative assessment of diffuse cerebral diseases by MRE.

REFERENCES

1. Linninger AA, Tsakiris C, Zhu DC, Xenos M, Roycewicz P, Danziger Z, Penn R. Pulsatile cerebrospinal fluid dynamics in the human brain. *IEEE Trans Biomed. Eng.* 2005; **52**(4): 557–565.
2. Pena A, Harris NG, Bolton MD, Czosnyka M, Pickard JD. Communicating hydrocephalus: the biomechanics of progressive ventricular enlargement revisited. *Acta Neurochir. Suppl.* 2002; **81**: 59–63.
3. Taylor Z, Miller K. Reassessment of brain elasticity for analysis of biomechanisms of hydrocephalus. *J. Biomech.* 2004; **37**(8): 1263–1269.
4. Bayly PV, Black EE, Pedersen RC, Leister EP, Genin GM. *In vivo* imaging of rapid deformation and strain in an animal model of traumatic brain injury. *J. Biomech.* 2006; **39**(6): 1086–1095.
5. Brands DW, Peters GW, Bovendeerd PH. Design and numerical implementation of a 3-D non-linear viscoelastic constitutive model for brain tissue during impact. *J. Biomech.* 2004; **37**(1): 127–134.
6. Pena A, Pickard JD, Stiller D, Harris NG, Schuhmann MU. Brain tissue biomechanics in cortical contusion injury: a finite element analysis. *Acta Neurochir. Suppl.* 2005; **95**: 333–336.
7. Kuroiwa T, Yamada I, Katsumata N, Endo S, Ohno K. *Ex vivo* measurement of brain tissue viscoelasticity in postischemic brain edema. *Acta Neurochir. Suppl.* 2006; **96**: 254–257.
8. Scholz M, Noack V, Pechlivanis I, Engelhardt M, Fricke B, Linstedt U, Brendel B, Ing D, Schmieder K, Ermert H, Harders A. Vibrography during tumor neurosurgery. *J. Ultrasound Med.* 2005; **24**(7): 985–992.
9. Choi AP, Zheng YP. Estimation of Young's modulus and Poisson's ratio of soft tissue from indentation using two different-sized indentors: finite element analysis of the finite deformation effect. *Med. Biol. Eng. Comput.* 2005; **43**(2): 258–264.
10. Miller K. Method of testing very soft biological tissues in compression. *J. Biomech.* 2005; **38**(1): 153–158.
11. Basford JR, Jenkyn TR, An KN, Ehman RL, Heers G, Kaufman KR. Evaluation of healthy and diseased muscle with magnetic resonance elastography. *Arch. Phys. Med. Rehabil.* 2002; **83**(11): 1530–1536.
12. Galban CJ, Maderwald S, Eggebrecht H, Grote W, de Greiff A, Uffmann K, Ladd ME. Monitoring the effects of chronic obstructive pulmonary disease on muscle elasticity by MR elastography. *Proceedings of the International Society of Magnetic Resonanc Medicine 13*. 2005; 2015.
13. Ringleb SI, Bensamoun SF, Chen Q, Manduca A, An KN, Ehman RL. Applications of magnetic resonance elastography to healthy and pathologic skeletal muscle. *J. Magn. Reson. Imaging.* 2007; **25**(2): 301–309.

DOI: 10.1002/nbm

14. Bercoff J, Chaffai S, Tanter M, Sandrin L, Catheline S, Fink M, Gennisson JL, Meunier M. *In vivo* breast tumor detection using transient elastography. *Ultrasound Med. Biol.* 2003; **29**(10): 1387–1396.
15. Cespedes I, Ophir J, Ponnekanti H, Maklad N. Elastography: elasticity imaging using ultrasound with application to muscle and breast *in vivo*. *Ultrason. Imaging.* 1993; **15**(2): 73–88.
16. Garra BS, Cespedes EI, Ophir J, Spratt SR, Zuurbier RA, Magnant CM, Pennanen MF. Elastography of breast lesions: initial clinical results. *Radiology* 1997; **202**(1): 79–86.
17. Itoh A, Ueno E, Tohno E, Kamma H, Takahashi H, Shiina T, Yamakawa M, Matsumura T. Breast disease: clinical application of US elastography for diagnosis. *Radiology* 2006; **239**(2): 341–350.
18. McKnight AL, Kugel JL, Rossman PJ, Manduca A, Hartmann LC, Ehman RL. MR elastography of breast cancer: preliminary results. *AJR Am. J. Roentgenol.* 2002; **178**(6): 1411–1417.
19. Thomas A, Fischer T, Frey H, Ohlinger R, Grunwald S, Blohmer JU, Winzer KJ, Weber S, Kristiansen G, Ebert B, Kummel S. Real-time elastography: an advanced method of ultrasound: first results in 108 patients with breast lesions. *Ultrasound Obstet. Gynecol.* 2006; **28**(3): 335–340.
20. Corpechot C, El Naggar A, Poujol-Robert A, Ziol M, Wendum D, Chazouilleres O, de Ledinghen V, Dhumeaux D, Marcellin P, Beaugrand M, Poupon R. Assessment of biliary fibrosis by transient elastography in patients with PBC and PSC. *Hepatology* 2006; **43**(5): 1118–1124.
21. Huwart L, Peeters F, Sinkus R, Annet L, Salameh N, ter Beek LC, Horsmans Y, Van Beers BE. Liver fibrosis: non-invasive assessment with MR elastography. *NMR Biomed.* 2006; **19**(2): 173–179.
22. Klatt D, Asbach P, Rump J, Papazoglou S, Somasundaram R, Modrow J, Braun J, Sack I. *In vivo* determination of hepatic stiffness using steady-state free precession magnetic resonance elastography. *Invest. Radiol.* 2006; **41**(12): 841–848.
23. Rouviere O, Yin M, Dresner MA, Rossman PJ, Burgart LJ, Fidler JL, Ehman RL. MR elastography of the liver: preliminary results. *Radiology* 2006; **240**(2): 440–448.
24. Sanada M, Ebara M, Fukuda H, Yoshikawa M, Sugiura N, Saisho H, Yamakoshi Y, Ohmura K, Kobayashi A, Kondoh F. Clinical evaluation of sonoelasticity measurement in liver using ultrasonic imaging of internal forced low-frequency vibration. *Ultrasound Med. Biol.* 2000; **26**(9): 1455–1460.
25. Ziol M, Handra-Luca A, Kettaneh A, Christidis C, Mal F, Kazemi F, de Ledinghen V, Marcellin P, Dhumeaux D, Trinchet JC, Beaugrand M. Noninvasive assessment of liver fibrosis by measurement of stiffness in patients with chronic hepatitis C. *Hepatology* 2005; **41**(1): 48–54.
26. Sinkus R, Tanter M, Catheline S, Lorenzen J, Kuhl C, Sondermann E, Fink M. Imaging anisotropic and viscous properties of breast tissue by magnetic resonance-elastography. *Magn. Reson. Med.* 2005; **53**(2): 372–387.
27. Xydeas T, Siegmann K, Sinkus R, Krainick-Strobel U, Miller S, Claussen CD. Magnetic resonance elastography of the breast: correlation of signal intensity data with viscoelastic properties. *Invest. Radiol.* 2005; **40**(7): 412–420.
28. Lewa CJ, De Certaines JD. Viscoelastic property detection by elastic displacement NMR measurements. *J. Magn. Reson. Imaging.* 1996; **6**(4): 652–656.
29. Muthupillai R, Lomas DJ, Rossman PJ, Greenleaf JF, Manduca A, Ehman RL. Magnetic resonance elastography by direct visualization of propagating acoustic strain waves. *Science* 1995; **269**(5232): 1854–1857.
30. Plewes DB, Betty I, Urchuk SN, Soutar I. Visualizing tissue compliance with MR imaging. *J. Magn. Reson. Imaging.* 1995; **5**(6): 733–738.
31. Kruse SA, Dresner MA, Rossman PJ, Felmlee JP, Jack CR, Ehman RL. Palpation of the brain using magnetic resonance elastography. *Proceedings of the International Society of Magnetic Resonanc Medicine 7*. 1999; 258.
32. McCracken PJ, Manduca A, Felmlee J, Ehman RL. Mechanical transient-based magnetic resonance elastography. *Magn. Reson. Med.* 2005; **53**(3): 628–639.
33. Uffmann K, Maderwald S, de Greiff A, Ladd M. Determination of gray and white matter elasticity with MR elastography. *Proceedings of the International Society of Magnetic Resonanc Medicine 12*. 2004; 1768.
34. Braun J, Bernarding J, Tolxdorff T, Sack I. *In vivo* magnetic resonance elastography of the human brain using ultrafast acquisition techniques. *Proceedings of the International Society of Magnetic Resonanc Medicine 10*. 2002; 2597.
35. Green M, Sinkus R, Cheng S, Bilston L. 3D MR-elastography of the brain at 3 tesla. *Proceedings of the International Society of Magnetic Resonanc Medicine 13*. 2005; 2176.
36. Hamhaber U, Sack I, Papazoglou S, Rump J, Klatt D, Braun J. Three-dimensional analysis of shear wave propagation observed by *in vivo* magnetic resonance elastography of the brain. *Acta Biomater.* 2007; **3**(1): 127–137.
37. Manduca A, Oliphant TE, Dresner MA, Mahowald JL, Kruse SA, Amromin E, Felmlee JP, Greenleaf JF, Ehman RL. Magnetic resonance elastography: non-invasive mapping of tissue elasticity. *Med. Image Anal.* 2001; **5**(4): 237–254.
38. Oliphant TE, Manduca A, Ehman RL, Greenleaf JF. Complex-valued stiffness reconstruction for magnetic resonance elastography by algebraic inversion of the differential equation. *Magn. Reson. Med.* 2001; **45**(2): 299–310.
39. Weaver JB, Van Houten EE, Miga MI, Kennedy FE, Paulsen KD. Magnetic resonance elastography using 3D gradient echo measurements of steady-state motion. *Med. Phys.* 2001; **28**(8): 1620–1628.
40. Barbone PE, Gokhale NH. Elastic modulus imaging: on the uniqueness and nonuniqueness of the elastography inverse problem in two dimensions. *Inverse Problems* 2004; **20**(1): 283–296.
41. Park E, Maniatty AM. Shear modulus reconstruction in dynamic elastography: time harmonic case. *Phys. Med. Biol.* 2006; **51**(15): 3697–3721.
42. Fung Y. *Biomechanics: Mechanical Properties of Living Tissue*. Springer-Verlag: New York, 1993.
43. Aki K, Richards PG. *Quantitative Seismology*. Universtiy Science Books: Sausalito, 2002.
44. Sandrin L, Fourquet B, Hasquenoph JM, Yon S, Fournier C, Mal F, Christidis C, Ziol M, Poulet B, Kazemi F, Beaugrand M, Palau R. Transient elastography: a new noninvasive method for assessment of hepatic fibrosis. *Ultrasound Med. Biol.* 2003; **29**(12): 1705–1713.
45. Catheline S, Wu F, Fink M. A solution to diffraction biases in sonoelasticity: the acoustic impulse technique. *J. Acoust. Soc. Am.* 1999; **105**(5): 2941–2950.
46. Papazoglou S, Rump J, Braun J, Sack I. Shear wave group velocity inversion in MR elastography of human skeletal muscle. *Magn. Reson. Med.* 2006; **56**(3): 489–497.
47. Nicolle S, Lounis M, Willinger R, Palierne JF. Shear linear behavior of brain tissue over a large frequency range. *Biorheology* 2005; **42**(3): 209–223.
48. Arbogast KB, Margulies SS. Regional differences in mechanical properties of the porcine central nervous system. *Proceedings of the 41st Stapp Car Crash Conference,* 1997; Lake Buena Vista, FL, USA.
49. Fallenstein GT, Hulce VD, Melvin JW. Dynamic mechanical properties of human brain tissue. *J. Biomech.* 1969; **2**(3): 217–226.
50. Shuck LZ, Advani SH. Rheological response of human brain tissue in shear. *ASME J. Basic. Eng.* 1972; **94**: 905–911.

DOI: 10.1002/nbm